

Robust linear correlations related to slope of nuclear symmetry energy

Y. Lei (雷杨),^{1,*} X. Lian (连新),² and C. L. Bai (白春林)^{2,†}

¹*School of Nuclear Science and Technology, Southwest University of Science and Technology, Mianyang 621010, China*

²*College of Physics, Sichuan University, Chengdu 610065, China*

(Dated: February 11, 2025)

With random interaction calculation, we observed the robust linear correlation between neutron skin thickness (ΔR_{np})/charge radius difference of mirror nuclei (ΔR_{mirr}) and the isospin asymmetry ($I = \frac{N-Z}{A}$). Shape coexistence is introduced to explain the obvious deviation of $^{18}\text{O}/\text{Ne}$ ΔR_{mirr} from the $\Delta R_{\text{mirr}} - I$ linearity. We also observe the slope of such linearity correlation (C_{np} or C_{mirr}) is also robustly and linearly correlated to the slope of the symmetry energy (L) against nucleon density at equilibrium density in the nuclear equation of state. Such linear correlation is further explained with intrinsic structural similarity between L and the symmetry energy coefficient (J). It is also adopted to constrain L to $20 \sim 36$ MeV. Considering the deviation of $^{18}\text{O}/\text{Ne}$ ΔR_{mirr} , the 1σ range of L is further reduced to $28 \sim 36$ MeV.

I. INTRODUCTION

Nuclear equation of state (EOS) is the fundamental ingredient for the description of the structure of neutron stars [1] and the dynamical evolution of binary compact-star mergers and core-collapse supernova, which provides the conditions of high densities and temperatures for nucleosynthesis beyond the iron group [2]. The density dependence of the nuclear symmetry energy in the EOS is also important in the study on drip lines, masses, densities, and collective excitations of neutron rich nuclei (for example, see [3–11]).

The neutron skin thickness ΔR_{np} , defined as the difference between the root-mean-squared radii of the neutron and proton density distributions, present the balance between the inward pressure of the surface tension on excess neutrons on the edge of the nucleus and outward degeneracy pressure from excess neutrons within the core of the nucleus, which is the same balance reached in neutron stars with the inward pressure of gravity. Therefore, the bulk property of neutron stars should be related to the neutron skin of nuclei [12–18].

More precisely, ΔR_{np} is believed to be positively and linearly correlated to the parameter L [19–21], the slope of the symmetry energy against nucleon density at equilibrium density. L at equilibrium density is critical for the extrapolation to high densities [22], under which these astrophysical objects and events can exist and emerge. For neutron stars, the amount of L , i.e., the softness or stiffness of EOS determines their radius [1]. In symmetric nuclear matter, L is proportional to the pressure of pure neutron matter at equilibrium density ρ_0 [23]. However, L cannot be directly determined by experiment. Therefore, one have to use data from terrestrial nuclear laboratory experiments and astrophysical observations to constrain L . For example, Chen *et al.* extracted $L = 88 \pm 25$ MeV out of isospin diffusion data in heavy-ion collisions

[24], Li *et al.* suggested $L = 58.9 \pm 16$ MeV with 29 previous analyses of terrestrial nuclear laboratory experiments and astrophysical observations [25]. Oertel *et al.* averaged over more than 53 results, and found $L = 58.7 \pm 28.1$ MeV [26]. A Bayesian approach was proposed to quantify the truncation errors from chiral effective field theory, and yielded $L = 59.8 \pm 4.1$ MeV at the 1σ level [27]. The neutron-star observations since the binary neutron star merger GW170817 also provided $L = 57.7 \pm 19$ MeV [28]. The results for L extracted from the pygmy dipole resonance in ^{68}Ni and ^{132}Sn were constrained to be in the intervals $50.3 \sim 89.4$ MeV and $29.0 \sim 82.0$ MeV [29], respectively. As suggested in Ref. [30], the slope parameter of the symmetry energy can be reduced to 37 ± 18 MeV by exploiting isovector giant quadrupole resonance energies.

Obviously, the correlation between ΔR_{np} and L is also valuable for constraining L with nuclear radius measurements. The general idea is choosing a certain many-body theory (mostly, Skyrme-Hatree-Fock model or covariant energy density functional theory), creating an ensemble with different interaction or energy density functional parametrizations for specific nucleus, whose experimental ΔR_{np} is currently available, and then quantitatively establishing the correlation between ΔR_{np} and L in such constructed ensemble, according to which the experimental ΔR_{np} provides L constrain.

Many effort has been devoted along this idea [31–36]. According to ΔR_{np} from the elastic scattering experiments of ^{208}Pb with longitudinally polarized electrons [37], relativistic energy density functionals suggested $L = 106 \pm 37$ MeV [38]. It significantly differs from the general L boundaries in Refs. [25–28], or even the L constrain from the neutron skin thickness of ^{48}Ca [39]. Nevertheless, what's the reasonable range of L , if the EOS is soft or stiff, and if the neutron star radii should be smaller or larger, are all still under debate.

Still the measurements of neutron radius are far difficult and inaccurate than those of proton one, since experimentalists are better at manipulating electromagnetic interaction, which is suitable for proton exploration, than strong or electroweak probes, which can be sensitive to

* leiyang19850228@gmail.com

† bclphy@scu.edu.cn

neutron density. Therefore, an alternative of ΔR_{np} is desirable for L constraint.

Wang, Li and Brown [16, 40] proposed the charge radii difference between mirror nuclei (ΔR_{mirr}) should also be correlated with L , considering that under absolute isospin conservation, $\Delta R_{\text{mirr}} = \Delta R_{\text{np}}$. Since ΔR_{mirr} only involves proton density probe, it may provide more precise data to constraint L . For example, from the charge radii of the mirror-partner nuclei $^{36}\text{Ca}/\text{S}$ and $^{38}\text{Ca}/\text{Ar}$, L is deduced to $5 \sim 70$ MeV [41]; from $^{54}\text{Ni}/\text{Fe}$, it's $21 \sim 88$ MeV [42]; a evaluation considering charge radius difference of all the three partners provide $L = 22.50 - 51.55$ MeV [43]; recent comprehensive survey also identified mirror pairs, which may be not suitable for L calibration [44].

Moreover, a linear correlation between ΔR_{np} (maybe ΔR_{mirr}) and the isospin asymmetry $I = \frac{N-Z}{A}$ was also noted (for example see Refs. [45–47]). As demonstrated in Fig. 1, except ΔR_{mirr} of $^{18}\text{O}/\text{Ne}$ pair, all the recently measured data of even-even nuclei follows this general linear correlation. Liquid drop model was frequently adopted to explain this linear correlation [21], where the slope of this proportional correlation corresponds to the ratio of the symmetry-energy coefficient J and the effective stiffness coefficient [47]. This proportional relation could be explained and also reproduced by mean field, *ab initio* coupled cluster and auxiliary field diffusion Monte Carlo models [47–51].

Thus, a many-body theory, which is governed by reasonable L , and thus provides experimentally consistent ΔR_{np} s or ΔR_{mirr} s for each nuclei with experimentally available data, should always provides this linear correlation between ΔR_{np} (or ΔR_{mirr}) and the isospin asymmetry $I = \frac{N-Z}{A}$ with experimentally consistent slope and intercept. Therefore, the existence, slope and intercept of the linear correlation in a many-body ensemble may also provide L constrain, which considers all available experimental ΔR_{np} or/and ΔR_{mirr} .

The first question raised should be "does the linear correlation between ΔR_{np} (or ΔR_{mirr}) and the isospin asymmetry $I = \frac{Z-N}{A}$ robustly exist in many-body theory ensembles, even without reasonable L , or well adjusted Hamiltonian?" We can see the many-body calculations [47–51] which brings this linear relation involve various interaction, model space, even theoretical frameworks. That may suggest that this correlation should be interaction and modeling detail irrelevant, and thus robust. However, such a linearity is actually not guaranteed at least in a microscopic point of view. Therefore, one should also test if this correlation is actually a robust simplicity out of complex many-body system, or requires specific or sophisticated interaction between nucleons.

Nuclear robust properties can mostly be demonstrated in an random interaction ensemble of nuclear structural model [63–66], where all the two-body or even one body interaction matrix elements are random numbers. With random interactions, one perform many-body calculations repeatedly. According to the resultant statistics,

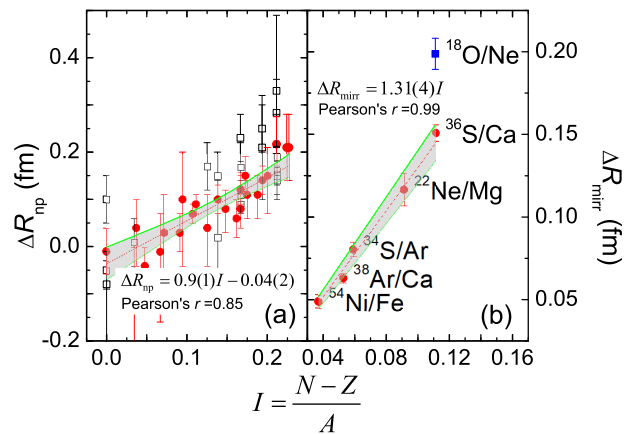


FIG. 1. (Color online) Experimental ΔR_{np} and ΔR_{mirr} against $I = \frac{N-Z}{A}$ of even-even nuclei, in Panel (a) and (b), respectively. In Panel (a), the most recent data we know [52–56] for each nucleus are demonstrated with red filled circles (\bullet), and others [52–54, 57–61] are shown with black open box (\square). Obviously, the recent ΔR_{np} remarkably converges to a linear relation to δ with Pearson's $r = 0.85$. A linear fitting is carried out for the recent ΔR_{np} data, resulting $\Delta R_{\text{np}} = 0.9(1)\delta - 0.04(2)$, as highlighted with gray shadowed 1σ -confidence band. In Panel (b), all the ΔR_{mirr} values are from Ref. [42, 45, 62]. Obvious linear correlation emerges with Pearson's $r = 0.99$ for all data except $^{18}\text{O}/\text{Ne}$ pair. Similarly to ^{208}Pb circumstance in Panel (a), $^{18}\text{O}/\text{Ne}$ data is highlighted with red open circle (\circ), considering its obvious deviation from general linear correlation. A proportional fitting is carried out for this general linear correlation, since $\Delta R_{\text{mirr}} \equiv 0$ for $\delta = 0$. Such a fitting provides $\Delta R_{\text{mirr}} = 1.31(4)\delta$, as highlighted with gray shadowed 1σ -confidence band.

the predominant patterns in random-interaction ensembles demonstrate how *simple* regularity emerges out of *complex* nuclei, even with interactions mostly deviating from reality [67]. Those regularities, for example, include $I^\pi = 0^+$ ground state predominance [68, 69], collective-motion likelihood [70, 71], odd-even staggering in proton-neutron interaction [72], nuclear observable correlations [73, 74].

II. $\Delta R_{\text{np}} - I$ AND $\Delta R_{\text{mirr}} - I$ LINEARITY

A. RQE calculation

To verify the robustness of the $\Delta R_{\text{np}} - I$ or $\Delta R_{\text{mirr}} - I$ linearity, we firstly decide to adopt the random quasiparticle ensemble (RQE) [68] without isospin symmetry, where the statistics of two-body interaction matrix elements stays invariant under particle-hole transformation, so that the shell-model calculations for all the nuclei within the model space are governed by the same interaction statistics properties, and thus guarantee a wider range of accessible δ in the RQE.

Secondly, we have to consider in which model space

we perform RQE calculations. Usual many-body calculation within a single major shell of harmonic oscillator always produce a constant expectation of \hat{r}^2 operator, i.e., zero ΔR_{np} . With two adjacent major shells, $\langle \hat{r}^2 \rangle$ is a linear combination of particle occupations of two shells, which may also lead to a trivial linearity of $\Delta R_{\text{np}} - \delta$ or $\Delta R_{\text{mirr}} - \delta$ correlation. In a microscopic view, nonlinear contribution of ΔR_{np} has to originate from the one-body correlation across two major shells, i.e., the nonzero nondiagonal matrix elements of $\langle nl|r^2|n'l \rangle$. For nuclei beyond *sd* shell or heavier, this nonlinear contribution can be negligible. Therefore, our shell-model calculations should be carried out in a single-particle model space with single-particle orbits from two major shell but with the same orbital angular momentum l , and total angular momentum j . More specifically, we perform our RQE calculations in spaces of $\{1d_{5/2}, 2d_{5/2}\}$, $\{1f_{7/2}, 2f_{7/2}\}$, $\{1h_{9/2}, 2h_{9/2}\}$, $\{1h_{11/2}, 2h_{11/2}\}$, $\{1j_{13/2}, 2j_{13/2}\}$, and $\{1j_{15/2}, 2j_{15/2}\}$, denoted by $d_{5/2}$, $f_{7/2}$, $h_{9/2}$, $h_{11/2}$, $j_{13/2}$ and $j_{15/2}$ in this paper.

Thirdly, within the RQE, we repeatedly perform more than 1000 shell-model calculations for each calculatable * pseudo nucleus in these model spaces, and obtain the $\langle \hat{r}_\pi^2 \rangle(Z, N)$ and $\langle \hat{r}_\nu^2 \rangle(Z, N)$ expectations of resultant ground states for proton or neutron distribution, respectively. Thus, $\Delta R_{\text{np}}(Z, N) = \sqrt{\langle \hat{r}_\nu^2 \rangle(Z, N)} - \sqrt{\langle \hat{r}_\pi^2 \rangle(Z, N)}$, and $\Delta R_{\text{mirr}}(Z, N) \simeq \sqrt{\langle \hat{r}_\pi^2 \rangle(N, Z)} - \sqrt{\langle \hat{r}_\pi^2 \rangle(Z, N)}$. Furthermore, we calculate the Pearson's r coefficient [76] between $\Delta R_{\text{np}}(Z, N)$ (or $\Delta R_{\text{mirr}}(Z, N)$) and $I = \frac{N-Z}{A}$ for each random interaction, in which case $|r| = 1$ means perfect linearity, and $|r| = 0$ suggests no linear correlation at all between the radius differences under investigation and isospin asymmetry δ . Then we perform counting for $|r|$ in each model space, and the probabilities of $|r| > 0.95$, $P(|r| > 0.95)$, are presented in Fig. 2, against the model-space sizes, which corresponds to the maximum nucleon number in each model space.

According to Fig. 2, all our RQE calculations could produce linear $\Delta R_{\text{np}} - \delta$ and $\Delta R_{\text{mirr}} - \delta$ correlations with $|r| > 0.95$ at a probability more than 1%. This percentage actually remarkably demonstrates the predominance of these two linear correlation within the RQE, considering that there would have been normally 10^{-5} order of possibility to produce $|r| > 0.95$, if our shell-model calculations provided independent random numbers as ΔR_{np} and ΔR_{mirr} outputs, according to our numerical experiments.

As increasing model size, we also note that $P(|r| > 0.95)$ increases dramatically for both $\Delta R_{\text{np}} - I$ and $\Delta R_{\text{mirr}} - I$ correlations, which suggests that as increasing

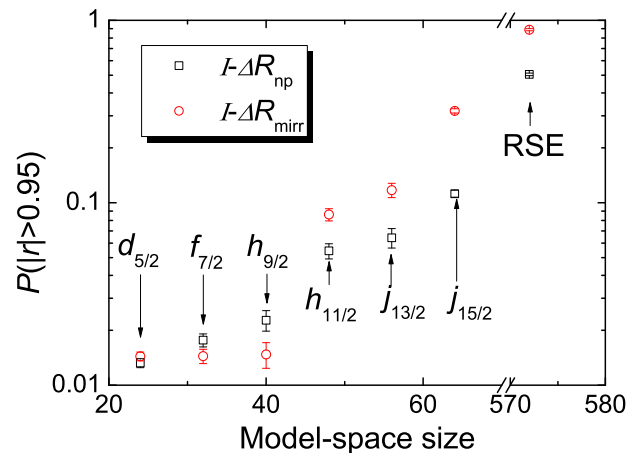


FIG. 2. (Color online) Probabilities of Pearson's $|r| > 0.95$, $P(|r| > 0.95)$, for $\Delta R_{\text{np}} - I$ and $\Delta R_{\text{mirr}} - I$ correlations, against model-space sizes within the RQE and RSE (random Skyrme ensemble) calculations. For RQE data, corresponding model-spaces are labeled, as well as for RSE calculations. The error bar corresponds to the statistic error of $|r|$ counting. According to our numerical test, if the our many-body calculations provided independent random number as ΔR_{np} and ΔR_{mirr} output, there would have been normally less than 10^{-5} order of possibility to produce $|r| > 0.95$, i.e., we would not have observed a single linear correlation within 10000 random-interaction runs.

the model size, the linearity of these two correlations become more pronounced. Such tendency is more obvious for $\Delta R_{\text{mirr}} - I$ correlation.

B. random Skyrme ensemble (RSE)

The model size of RQE calculations is limited, due to the heavy burden of shell-model computation. For further exploration, we introduce the Skyrme-Hartree-Fock (denoted by SHF) calculations with lowest 10 major shells of isotropic harmonic oscillator, to enlarge the model space of our many-body calculations. Corresponding model space includes 572 single-particle levels, which is far more than the shell-model spaces dose in our RQE calculations. The SHF calculation is performed with the HFBTHO code [77], by switching off the zero-range pairing interactions.

We collect 160 previously proposed Skyrme parametrizations mostly listed in Ref. [78], for such calculations, and perform SHF calculations for all the nuclei involved in Fig. 1, as well as ^{22}Si , ^{26}S , ^{30}Ar , ^{34}Ca , ^{38}Ti , ^{28}S , and ^{50}Ni , which was also introduced to extend the range of I for the investigation on the linear correlation of $\Delta R_{\text{mirr}} - I$ in Ref. [47]. Such calculations constructed a many-body ensemble we call ‘‘Skyrme ensemble’’.

In the Skyrme ensemble, we observed strong linearity of $\Delta R_{\text{np}} - I$ correlation and $\Delta R_{\text{mirr}} - I$ with Pearson's $r > 0.85$, for *all* the parametrizations, which agrees with

* ‘‘Calculatable’’ means the shell-model calculation for a specific pseudo nuclei takes no more than 64GB memory with a 36-thread openmp run of BIGSTICK [75].

experiments demonstrated in Fig. 1. We also note that in Skyrme ensemble, the Pearson's r values of $\Delta R_{\text{np}} - I$ correlation are generally smaller than those of $\Delta R_{\text{mirr}} - I$, which agrees with our observation with the RQE in Fig. 2, that the linearity of $\Delta R_{\text{mirr}} - I$ correlation could become more pronounced with larger model space.

As we have argued that such large possibility with r close to 1 may suggest a possible interaction independent property of quantum many-body system governed by Skyrme force. To test this argument, we further randomize the Skyrme parametrizations here. A general Skyrme force includes 10 parameters ($t_{0\sim 3}$, $x_{0\sim 3}$, W_0 and $1/\sigma$), as described in Eq. (2) of Ref. [43]. For the 160 Skyrme parametrizations we introduced in the Skyrme ensemble, these 10 parameters' mean values and have covariance matrix are provided in Table I. According to the algorithm provide in Ref. [79], we used linear transformations of independent Gaussian random number to generate random Skyrme parametrizations with similar means, fluctuations and correlation to those of the 160 Skyrme parameters listed in Table I.

Beside the consideration of statistic nature of random Skyrme parameters, we also need to make sure the existence of the nuclear matter governed by such randomized Skyrme force, which may be demonstrated by corresponding saturation density (ρ_0). Unlike 160 Skyrme parametrizations in the Skyrme ensemble, which were well adjusted targeting realistic nuclear properties, the random Skyrme parametrization dose not necessarily provide ρ_0 close to 0.16 fm^{-3} , i.e., the realistic value. The density should be the root of saturation condition equation of

$$\frac{\hbar^2}{5m} \left(\frac{3\pi^2}{2} \right)^{2/3} \rho_0^{-1/3} + \frac{3}{8}t_0 + \frac{1}{16}t_3(\alpha + 1)\rho_0^\alpha + \frac{1}{16} [3t_1 + t_2 (5 + 4x_2)] \left(\frac{3\pi^2}{2} \right)^{2/3} \rho_0^{2/3} = 0 \quad (1)$$

If a certain Skyrme parametrization provide a saturation condition equation without positive real solution of ρ_0 , that means no nuclear matter could exist under such a Skyrme force. We believe such a parametrization is too nonphysical, and thus neglected in our following ensemble investigation.

We also remind this work aims to serve the L constrain. To fairly investigate the predominance of linear $\Delta R_{\text{np}} - I$ and $\Delta R_{\text{mirr}} - I$ correlations for different L values, and to exclude the non-unified background of L from the random Skyrme calculations, we sample about 4000 Skyrme parametrizations for each $\Delta L = 5$ interval in $L = 0 \sim 200$ MeV range, where L is obtained at the saturation density ρ_0 from Eq. (1). Then, we further introduced them into the SHF calculations for nuclei involved in Fig. 1, as well as ^{22}Si , ^{26}S , ^{30}Ar , ^{34}Ca , ^{38}Ti , ^{28}S , and ^{50}Ni . To save computational time, we adopt initial single-particle basis with a prolate deformation of $\beta = 0.2$, which highly possible to produce a prolate HF solution. Such random interaction calcula-

tions constructs a random Skyrme ensemble (denoted by RSE in this paper). For each parametrization, we calculate Pearson's r of $\Delta R_{\text{np}} - I$ and $\Delta R_{\text{mirr}} - I$ correlations, and find 50.6(9)% and 89(1)% possibility to have strong linearity with $r > 0.95$, respectively. Such large possibilities are even more remarkable than that from our RQE calculations. For comparison, We also plot these two percentages into Fig. 2. The large model size of SHF calculation indeed strengths the predominance of linear $\Delta R_{\text{np}} - I$ and $\Delta R_{\text{mirr}} - I$ correlations.

For realistic nuclear system, the nucleons move in infinite Hilbert space. According to our observation in Fig. 2, robust linear correlations of $\Delta R_{\text{np}} - I$ or $\Delta R_{\text{mirr}} - I$ definitely are expected, as we have observed in experiments as shown in Fig. 1.

III. $C_{\text{np}} - L$ AND $C_{\text{mirr}} - L$ LINEARITY

Since we successfully establish the robust linearity of $\Delta R_{\text{np}} - I$ or $\Delta R_{\text{mirr}} - I$ correlation, and we are also aware of that ΔR_{np} and ΔR_{mirr} should also be linearly correlated to the symmetry energy slope L , we expect the slope of the $\Delta R_{\text{np}} - I$ or $\Delta R_{\text{mirr}} - I$ correlations (denoted by C_{np} and C_{mirr} , respectively) is also linearly correlated to L .

A. verification

Now we test this conjecture in the Skyrme ensemble, where 160 previously proposed Skyrme parametrizations are included. Since all the Skyrme parametrizations bring Pearson's $r > 0.85$ for the $\Delta R_{\text{np}} - I$ or $\Delta R_{\text{mirr}} - I$ correlations, as we found, we can safely perform linear fitting for $\Delta R_{\text{np}} - I$ correlation and proportional fitting for $\Delta R_{\text{mirr}} - I$, considering that $\Delta R_{\text{mirr}} \equiv 0$ for $I = 0$. The residual of such fitting should be reasonably small, guaranteed by close 1 Pearson's r . We plot resultant C_{np} and C_{mirr} against L at ρ_0 for each parametrizations in the Skyrme ensemble, as shown in Fig. 3. The linearity is obvious in the $C_{\text{np}} - L$ and $C_{\text{mirr}} - L$ correlations. We also note that for small $L < 100$ MeV, C_{np} is systematically smaller than C_{mirr} , and as increasing L , the difference between C_{np} and C_{mirr} gradually vanishes.

We can also observe the linear correlation of $C_{\text{np}} - L$ and $C_{\text{mirr}} - L$ in the RSE. For all the Skyrme parametrizations in the RSE with Pearson's r larger than 0.85, we perform two-dimensional counting of $\{C_{\text{np}}, L\}$ and $\{C_{\text{mirr}}, L\}$ data pair. The counting results are presented in Fig. 4 with gray mapping. As show in Fig. 4(a), there exists obvious linear correlation between c_{np} and L . However, in Fig. 4(b), such a linear correlation preserves for $L < 140$ MeV, and after crossing $L = 140$ MeV, the slope of the linearity becomes smaller. Similarly to that in the Skyrme ensemble with well adjusted Skyrme parametrizations, for small $L < 100$ MeV, C_{np} is systematically smaller than C_{mirr} , while for larger L they are

TABLE I. Mean values and covariance matrix of the 160 Skyrme parametrizations in the Skyrme ensemble. The notation of Skyrme parameters follow Eq. (2) of Ref. [43].

	$\langle t_0 \rangle$	$\langle t_1 \rangle$	$\langle t_2 \rangle$	$\langle t_3 \rangle$	$\langle x_0 \rangle$	$\langle x_1 \rangle$	$\langle x_2 \rangle$	$\langle x_3 \rangle$	$\langle W_0 \rangle$	$\langle 1/\sigma \rangle$
mean	-2.03×10^3	394	-156	1.3×10^4	0.443	-0.461	0.471	0.594	134	4.11
covariance	t_0	t_1	t_2	t_3	x_0	x_1	x_2	x_3	W_0	$1/\sigma$
t_0	2.39×10^5	-1.21×10^4	4.26×10^4	-5.39×10^5	-29.5	18.6	247	-86.3	-2.95×10^3	-821
t_1	-1.21×10^4	1.32×10^4	276	-1.52×10^5	0.6	-12.3	-33.1	14	1.21×10^3	65.2
t_2	4.26×10^4	276	1.41×10^5	-2.56×10^5	-77.8	-229	119	-124	4.97×10^3	-140
t_3	-5.39×10^5	-1.52×10^5	-2.56×10^5	8.35×10^6	157	373	-1.22×10^3	49.8	-1.54×10^4	1.49×10^3
x_0	-29.5	0.6	-77.8	157	0.146	0.0574	-0.114	0.241	-0.399	0.134
x_1	18.6	-12.3	-229	373	0.0574	0.688	-0.046	5.04×10^{-3}	-17.9	-0.12
x_2	247	-33.1	119	-1.22×10^3	-0.114	-0.046	46	-0.176	-7.23	-1.01
x_3	-86.3	14	-124	49.8	0.241	5.04×10^{-3}	-0.176	0.484	4.04	0.375
W_0	-2.95×10^3	1.21×10^3	4.97×10^3	-1.54×10^4	-0.399	-17.9	-7.23	4.04	1.82×10^3	13.2
$1/\sigma$	-821	65.2	-140	1.49×10^3	0.134	-0.12	-1.01	0.375	13.2	2.99

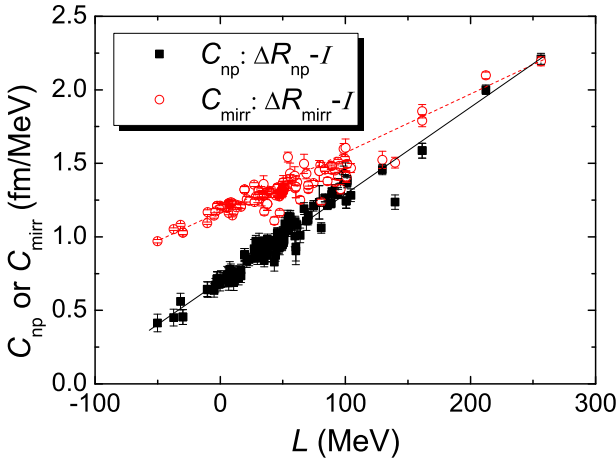


FIG. 3. (Color online) Slope of the $\Delta R_{np} - I$ and $\Delta R_{mirr} - I$ linear correlation (C_{np} and C_{mirr} , respectively) against L at ρ_0 in the Skyrme ensemble, where 160 previously proposed Skyrme parametrizations are included. General linear correlation for both $c_{np} - L$ and $c_{mirr} - L$ correlations are obvious, as highlighted by the eye-guided black solid and red dash lines.

quantitatively comparable to each other.

B. explanation

Now let's understand why there exists robust linear correlations of $C_{np} - L$ and $C_{mirr} - L$. Since ΔR_{mirr} is just an alternative of ΔR_{np} , we focus on $C_{np} - L$ and take the robustness of linear $C_{mirr} - L$ as a representation of linearity of $C_{np} - L$ correlation. We follow the formalism from the supplement of Ref. [47], where

$$C_{np} = \frac{3}{2} r_0 \frac{J}{Q^*}, \quad (2)$$

and J is the symmetry energy coefficient, r_0 is oscillation parameter, Q^* is the effective surface stiffness coefficient, describing the stiffness against the pulling apart of neutrons and protons in the surface. With Skyrme energy

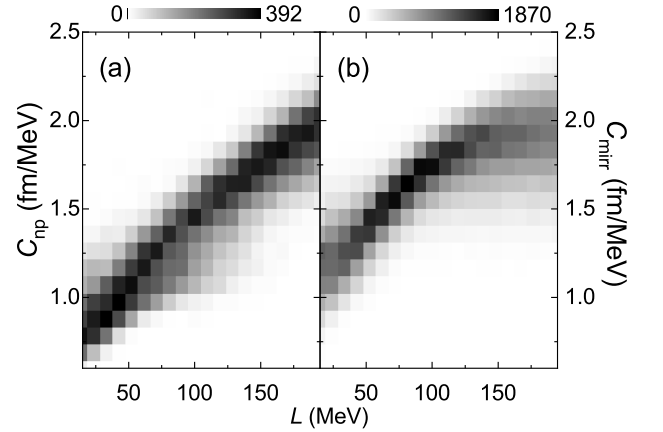


FIG. 4. Grey mapped two denominational counting of C_{np}, L and C_{mirr}, L in the random Skyrme ensemble (RSE). C_{np} and C_{mirr} are calculated with corresponding Pearson's $r > 0.85$. Similarity to Fig. 3, robust linear correlation for both $C_{np} - L$ and $C_{mirr} - L$ correlations are observed.

density functional, J and Q^* are also functions of Skyrme parametrization, like L . Moreover, we also note that Q^* actually is related with specific N and Z numbers within the many-body calculations (for example in Ref. [80]). Since the linear correlation of $\Delta R_{np} - L$ is robust across the whole nuclide chart, one have to expect C_{np} is numerically stable against N and Z numbers, which further suggest the N and Z -dependence of Q^* should not affect C_{np} too much. Thus, following Ref. [47] we can take Q^* roughly as a constant, without loss of generality. Thus, if C_{np} and L are linearly correlated, there should exists $J - L$ linear correlation according to Eq. (2) in the L range, where we observed the $C_{np} - L$ linearity in Fig. 3 and 4(a). To verify the linearity of $J - L$ correlation, in the Skyrme ensemble with 160 parametrizations, we plot

J calculated with

$$\begin{aligned}
 J &= J_1 + J_2 + J_3 + J_4 \\
 J_1 &= \frac{\hbar^2}{6m} c \rho^{2/3} \\
 J_2 &= -\frac{1}{8} t_0 (1 + 2x_0) \rho \\
 J_3 &= -\frac{1}{48} t_3 (1 + 2x_3) \rho^{\alpha+1} \\
 J_4 &= -\frac{1}{24} [3t_1 x_1 - t_2 (4 + 5x_2)] c \rho^{5/3}
 \end{aligned} \tag{3}$$

against L calculated with

$$L = 2J_1 + 3J_2 + 4(1 + \sigma)J_3 + 5J_4 \tag{4}$$

in Fig. 5(a). There exists some fluctuation of the $J - L$ correlation for $L < 50$ MeV, while for $L = 50 \sim 300$ MeV, the $J - L$ linearity roughly emerges. In the RSE, we repeat similar calculations, and perform two-dimensional counting of $\{J, L\}$ sets within the RSE ensemble, as presented in Fig. 5(b), similar observation about the $J - L$ linearity emerges.

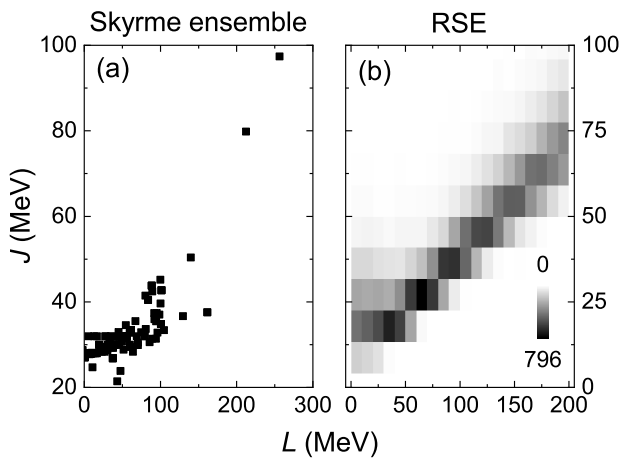


FIG. 5. J against L in the Skyrme ensemble and RSE ensemble, as shown in Panel (a) and (b) respectively. In (b) gray mapped two-dimensional counting is presented for $\{J, L\}$ combinations, since there are about 150000 J, L combinations in the RSE, which is too much for directly plotting.

Now the question becomes why L and J tend to be linear correlated. Let take a close look at the J and L calculations in Eqs. (3) and (4). One can see that L and J are both linear combination of $L_1, L_2, L_3,$ and L_4 . According to our numerical experiment, if L_1, L_2, L_3, L_4 and σ are all independent random numbers of normal distribution, the percentage of Pearson's $r > 0.9$ between ten J and L values calculated according to Eqs. (3) and (4) is 49(2)%. While, if J and L are independent random numbers of normal distribution, such a percentage is only 1.90(4)%. The similarity in the structure of linear combination between L and J shown in Eqs. (3) and (4) obviously increases the linearity between L and J , i.e., L and C_{np} . That may partially explain the robust linear correlation in Figs. 3 and 4.

IV. L CONSTRAINT

A. according to $C_{\text{np}} - L$ and $C_{\text{mirr}} - L$ correlation

The linear correlation of $C_{\text{np}} - L$ and $C_{\text{mirr}} - L$ could be important for L constrain. First of all, experimental C_{np} is obviously smaller than C_{mirr} according to Fig. 1, which suggest that L can't be larger than 100 MeV, where $C_{\text{np}} \simeq C_{\text{mirr}}$. Secondly, the linearity of $C_{\text{np}} - L$ and $C_{\text{mirr}} - L$ correlations is very robust, and corresponding slope are large enough to make C_{np} and C_{mirr} very sensitive to L . Therefore, the robust linear $C_{\text{np}} - L$ and $C_{\text{mirr}} - L$ correlations also provide quantitative constrain on L , given experimental $C_{\text{np}} = 0.9(1)$ fm/MeV and $C_{\text{mirr}} = 1.31(4)$ fm/MeV. Such constrain gives full consideration of all available experimental neutron skins or charge radius differences between mirror nuclei, and thus may provide more strict constrain on L than previous constraints from a single neutron skin measurement, or charge radius of only one mirror pair.

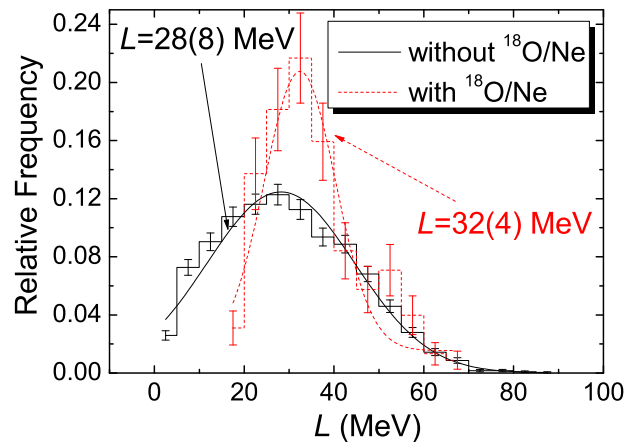


FIG. 6. (Color online) L distributions of two sample sets of Skyrme parametrizations out of the RSE. The black solid lines correspond the parametrizations, which could reproduce the linearity of $\Delta R_{\text{np}} - I$ and $\Delta R_{\text{mirr}} - I$ with Pearson's $r > 0.85$ and 0.99 respectively, and corresponding C_{np} and C_{mirr} within experimental error. The red dash lines correspond those, which additionally reproduce ΔR_{mirr} of $^{18}\text{O}/\text{Ne}$ mirror pair within experimental error, considering possible shape coexistence of ^{18}O . The step lines are from sample counting, with error bar from statistical error estimation. The curves correspond to asymmetric Gaussian fitting as described by Eq. (??), which gives constraints on $L = 26_{-7}^{+9}$ MeV and 35_{-4}^{+7} MeV with and without considering ΔR_{mirr} of $^{18}\text{O}/\text{Ne}$ mirror pair, respectively.

More precisely, we sample the Skyrme parametrizations in the RSE, which could reproduce the linearity of $\Delta R_{\text{np}} - I$ and $\Delta R_{\text{mirr}} - I$ with Pearson's $r > 0.85$ and 0.99 respectively, and corresponding C_{np} and C_{mirr} within experimental error. The L distribution of these sampled parametrization demonstrate the reasonable range of L . In Fig. 6, the black solid step line presents such a distribution. The distribution brings an peak, which can be

fitted by an Gaussian function. The fitting curve is presented in Fig. 6 with black solid line with peak center at 28.2 and width 16.4. Thus, according to the experimental slope of $\Delta R_{\text{np}} - I$ and $\Delta R_{\text{mirr}} - I$, $L = 28_{-8}^{+8}$ MeV with 1σ confidence.

B. considering $^{18}\text{O}/\text{Ne}$ mirror pair

Since there is robust linearity of $\Delta R_{\text{mirr}} - I$ correlation, if we sample the Skyrme parametrizations, which could reproduce the linearity of $\Delta R_{\text{mirr}} - I$, then those parametrizations should unlikely reproduce $^{18}\text{O}/\text{Ne}$ ΔR_{np} consistent with experiments. We tried to sample Skyrme parametrizations, which could reproduce linear $\Delta R_{\text{np}} - I$ and $\Delta R_{\text{mirr}} - I$ with experimental slopes, as well as $^{18}\text{O}/\text{Ne}$ ΔR_{np} . Out of ~ 150000 parametrizations in the RSE, we find none fit such sample criteria.

How do we understand the obvious deviation of $^{18}\text{O}/\text{Ne}$ mirror pair in Fig. 1? First of all, we remind that the $^{18}\text{O}/\text{Ne}$ is well known candidates with shape coexistence [81]. Recently survey also suggests that the coexistence could be pervasive across the whole nuclide chart. [82]. Secondly, as we have stated, we start our SHF calculation from $\beta = 0.2$ initial basis, which likely only converges to a single prolate deformation. It's possible that the shape coexistence of $^{18}\text{O}/\text{Ne}$ pair creates multiplet of ΔR_{mirr} , one of which follows the robust linearity of $\Delta R_{\text{mirr}} - I$, and another of which agrees with the experimental ΔR_{mirr} of $^{18}\text{O}/\text{Ne}$.

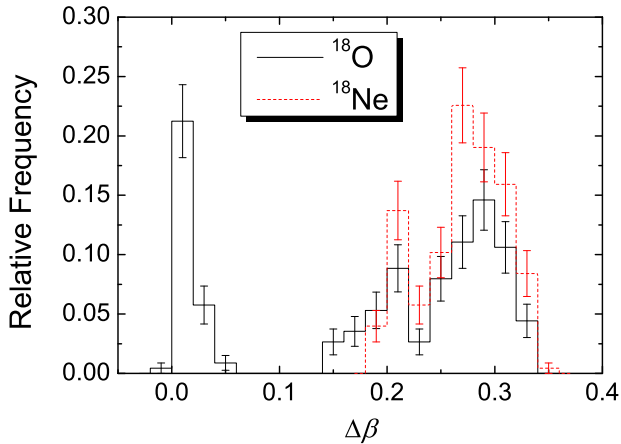


FIG. 7. (Color online) Distributions of β differences ($\Delta\beta$) of ^{18}O and ^{18}Ne between two scenarios, one of which follows the experimental $\Delta R_{\text{mirr}} - I$ linearity, and one of which reproduces the experimental ΔR_{mirr} of $^{18}\text{O}/\text{Ne}$ for selected parametrizations in the RSE with shape coexistence consideration. None-zero $\Delta\beta$ corresponds to shape coexistence.

To verify this shape coexistence picture, we repeat our RSE calculations starting from basis with $\beta = -0.2 \sim 0.2$ with 0.01 interval for $^{18}\text{O}/\text{Ne}$. Obviously, for each parametrizations, one can obtain different ΔR_{mirr} values for $^{18}\text{O}/\text{Ne}$. We collect the parametrizations, which could produce both ΔR_{mirr} value fitting the experimental $\Delta R_{\text{mirr}} - I$ linearity, and ΔR_{mirr} value consistent with the experimental ΔR_{mirr} of $^{18}\text{O}/\text{Ne}$. Out of ~ 150000 parametrization, there are ~ 200 , which fits the above criteria. For these ~ 200 parametrizations, we calculate the β differences ($\Delta\beta$) of ^{18}O and ^{18}Ne between two scenarios, one of which follows the experimental $\Delta R_{\text{mirr}} - I$ linearity, and one of which reproduces the experimental ΔR_{mirr} of $^{18}\text{O}/\text{Ne}$. We plot the distribution of the resultant β differences in Fig. 7. For ^{18}O , there are three peaks around $\Delta\beta \sim 0$, 0.2 and 0.3, corresponding to no shape coexistence, spherical-deformed coexistence between $\beta \simeq 0$ and ± 0.2 , and prolate-oblate coexistence between $\beta \simeq 0.2$ and -0.1 , or $\beta \simeq 0.1$ and -0.2 . For ^{18}Ne , two peaks locate at $\Delta\beta \sim 0.2$ and 0.3, suggesting spherical-deformed and prolate-oblate coexistence. Thus, to reproduce $\Delta R_{\text{mirr}} - I$ linearity and ΔR_{mirr} of $^{18}\text{O}/\text{Ne}$ within the same Skyrme parametrization, one has to introduce shape coexistence for $^{18}\text{O}/\text{Ne}$ mirror pair.

Finally, we can also set constrain on L with above sampled skyrme parametrization with considering the $^{18}\text{O}/\text{Ne}$ ΔR_{mirr} experimental fitness. We also plot the L distribution of these parametrizations in Fig. 6, and the Gaussian fit suggests $L = 32(4)$ MeV.

V. SUMMARY

With random interaction calculation, we observed the robust linear correlation between neutron skin thickness (ΔR_{np})/charge radius difference of mirror nuclei (ΔR_{mirr}) and the isospin asymmetry ($I = \frac{N-Z}{A}$). Shape coexistence is introduced to explain the obvious deviation of $^{18}\text{O}/\text{Ne}$ ΔR_{mirr} from the $\Delta R_{\text{mirr}} - I$ linearity. We also observe the slope of such linearity correlation (C_{np} or C_{mirr}) is also robustly and linearly correlated to the slope of the symmetry energy (L) against nucleon density at equilibrium density in the nuclear equation of state. Such linear correlation is further explained with intrinsic structural similarity between L and the symmetry energy coefficient (J). It is also adopted to constrain L to $20 \sim 36$ MeV. Considering the deviation of $^{18}\text{O}/\text{Ne}$ ΔR_{mirr} , the 1σ range of L is further reduced to $28 \sim 36$ MeV.

[1] J. M. Lattimer and M. Prakash, Neutron star observations: Prognosis for equation of state constraints, *Physics*

- ume 1906-2006.
- [2] M. Oertel, M. Hempel, T. Klähn, and S. Typel, Equations of state for supernovae and compact stars, *Rev. Mod. Phys.* **89**, 015007 (2017).
 - [3] B. Alex Brown, Neutron radii in nuclei and the neutron equation of state, *Phys. Rev. Lett.* **85**, 5296 (2000).
 - [4] S. Typel and B. A. Brown, Neutron radii and the neutron equation of state in relativistic models, *Phys. Rev. C* **64**, 027302 (2001).
 - [5] R. Furnstahl, Neutron radii in mean-field models, *Nuclear Physics A* **706**, 85 (2002).
 - [6] A. Steiner, M. Prakash, J. Lattimer, and P. Ellis, Isospin asymmetry in nuclei and neutron stars, *Physics Reports* **411**, 325 (2005).
 - [7] B. G. Todd-Rutel and J. Piekarewicz, Neutron-rich nuclei and neutron stars: A new accurately calibrated interaction for the study of neutron-rich matter, *Phys. Rev. Lett.* **95**, 122501 (2005).
 - [8] M. Centelles, X. Roca-Maza, X. Viñas, and M. Warda, Nuclear symmetry energy probed by neutron skin thickness of nuclei, *Phys. Rev. Lett.* **102**, 122502 (2009).
 - [9] M. Warda, X. Viñas, X. Roca-Maza, and M. Centelles, Neutron skin thickness in the droplet model with surface width dependence: Indications of softness of the nuclear symmetry energy, *Phys. Rev. C* **80**, 024316 (2009).
 - [10] A. Carbone, G. Colò, A. Bracco, L.-G. Cao, P. F. Bortignon, F. Camera, and O. Wieland, Constraints on the symmetry energy and neutron skins from pygmy resonances in ^{68}Ni and ^{132}Sn , *Phys. Rev. C* **81**, 041301 (2010).
 - [11] L.-W. Chen, C. M. Ko, B.-A. Li, and J. Xu, Density slope of the nuclear symmetry energy from the neutron skin thickness of heavy nuclei, *Phys. Rev. C* **82**, 024321 (2010).
 - [12] B. Alex Brown, Neutron radii in nuclei and the neutron equation of state, *Phys. Rev. Lett.* **85**, 5296 (2000).
 - [13] C. J. Horowitz and J. Piekarewicz, Neutron star structure and the neutron radius of ^{208}Pb , *Phys. Rev. Lett.* **86**, 5647 (2001).
 - [14] M. B. Tsang, J. R. Stone, F. Camera, P. Danielewicz, S. Gandolfi, K. Hebeler, C. J. Horowitz, J. Lee, W. G. Lynch, Z. Kohley, R. Lemmon, P. Möller, T. Murakami, S. Riordan, X. Roca-Maza, F. Sammarruca, A. W. Steiner, I. Vidaña, and S. J. Yennello, Constraints on the symmetry energy and neutron skins from experiments and theory, *Phys. Rev. C* **86**, 015803 (2012).
 - [15] G. Hagen, A. Ekström, C. Forssén, G. R. Jansen, W. Nazarewicz, T. Papenbrock, K. A. Wendt, S. Bacca, N. Barnea, B. Carlsson, C. Drischler, K. Hebeler, M. Hjorth-Jensen, M. Miorelli, G. Orlandini, A. Schwenk, and J. Simonis, Neutron and weak-charge distributions of the ^{48}Ca nucleus, *Nature Physics* **12**, 186 (2016).
 - [16] B. A. Brown, Mirror charge radii and the neutron equation of state, *Phys. Rev. Lett.* **119**, 122502 (2017).
 - [17] F. J. Fattoyev, J. Piekarewicz, and C. J. Horowitz, Neutron skins and neutron stars in the multimessenger era, *Phys. Rev. Lett.* **120**, 172702 (2018).
 - [18] C. A. Bertulani and J. Valencia, Neutron skins as laboratory constraints on properties of neutron stars and on what we can learn from heavy ion fragmentation reactions, *Phys. Rev. C* **100**, 015802 (2019).
 - [19] X. Roca-Maza, M. Centelles, X. Viñas, and M. Warda, Neutron skin of ^{208}Pb , nuclear symmetry energy, and the parity radius experiment, *Phys. Rev. Lett.* **106**, 252501 (2011).
 - [20] P.-G. Reinhard and W. Nazarewicz, Nuclear charge and neutron radii and nuclear matter: Trend analysis in skyrme density-functional-theory approach, *Phys. Rev. C* **93**, 051303 (2016).
 - [21] A. Steiner, M. Prakash, J. Lattimer, and P. Ellis, Isospin asymmetry in nuclei and neutron stars, *Physics Reports* **411**, 325 (2005).
 - [22] B. Alex Brown, Neutron radii in nuclei and the neutron equation of state, *Phys. Rev. Lett.* **85**, 5296 (2000).
 - [23] B. A. Brown, Mirror charge radii and the neutron equation of state, *Phys. Rev. Lett.* **119**, 122502 (2017).
 - [24] L.-W. Chen, C. M. Ko, and B.-A. Li, Nuclear matter symmetry energy and the neutron skin thickness of heavy nuclei, *Phys. Rev. C* **72**, 064309 (2005).
 - [25] B.-A. Li and X. Han, Constraining the neutron-proton effective mass splitting using empirical constraints on the density dependence of nuclear symmetry energy around normal density, *Physics Letters B* **727**, 276 (2013).
 - [26] M. Oertel, M. Hempel, T. Klähn, and S. Typel, Equations of state for supernovae and compact stars, *Rev. Mod. Phys.* **89**, 015007 (2017).
 - [27] C. Drischler, R. J. Furnstahl, J. A. Melendez, and D. R. Phillips, How well do we know the neutron-matter equation of state at the densities inside neutron stars? a bayesian approach with correlated uncertainties, *Phys. Rev. Lett.* **125**, 202702 (2020).
 - [28] B.-A. Li, B.-J. Cai, W.-J. Xie, and N.-B. Zhang, Progress in constraining nuclear symmetry energy using neutron star observables since gw170817, *Universe* **7**, 10.3390/universe7060182 (2021).
 - [29] A. Carbone, G. Colò, A. Bracco, L.-G. Cao, P. F. Bortignon, F. Camera, and O. Wieland, Constraints on the symmetry energy and neutron skins from pygmy resonances in ^{68}Ni and ^{132}Sn , *Phys. Rev. C* **81**, 041301 (2010).
 - [30] X. Roca-Maza, M. Brenna, B. K. Agrawal, P. F. Bortignon, G. Colò, L.-G. Cao, N. Paar, and D. Vretenar, Giant quadrupole resonances in ^{208}Pb , the nuclear symmetry energy, and the neutron skin thickness, *Phys. Rev. C* **87**, 034301 (2013).
 - [31] Z. Zhang and L.-W. Chen, Constraining the symmetry energy at subsaturation densities using isotope binding energy difference and neutron skin thickness, *Physics Letters B* **726**, 234 (2013).
 - [32] C. Mondal, B. K. Agrawal, M. Centelles, G. Colò, X. Roca-Maza, N. Paar, X. Viñas, S. K. Singh, and S. K. Patra, Model dependence of the neutron-skin thickness on the symmetry energy, *Phys. Rev. C* **93**, 064303 (2016).
 - [33] L. Min, L. Zhu-Xia, W. Ning, and Z. Feng-Shou, Exploring nuclear symmetry energy with isospin dependence in neutron skin thickness of nuclei, *Chinese Physics C* **35**, 629 (2011).
 - [34] X. Fan, J. Dong, and W. Zuo, Symmetry energy at subsaturation densities and the neutron skin thickness of ^{208}Pb , *Science China Physics, Mechanics & Astronomy* **58**, 1 (2015).
 - [35] C. Xu, Z. Ren, and J. Liu, Attempt to link the neutron skin thickness of ^{208}Pb with the symmetry energy through cluster radioactivity, *Phys. Rev. C* **90**, 064310 (2014).
 - [36] J. Xu, W.-J. Xie, and B.-A. Li, Bayesian inference of nuclear symmetry energy from measured and imagined neutron skin thickness in $^{116,118,120,122,124,130,132}\text{Sn}$, ^{208}Pb , (2011).

- and ^{48}Ca , *Phys. Rev. C* **102**, 044316 (2020).
- [37] D. Adhikari, H. Albatineh, D. Androic, K. Aniol, D. S. Armstrong, T. Averett, C. Ayerbe Gayoso, S. Barcus, V. Bellini, R. S. Beminiwattha, J. F. Benesch, H. Bhatt, D. Bhatta Pathak, D. Bhetuwal, B. Blaikie, Q. Campagna, A. Camsonne, G. D. Cates, Y. Chen, C. Clarke, J. C. Cornejo, S. Covrig Dusa, P. Datta, A. Deshpande, D. Dutta, C. Feldman, E. Fuchey, C. Gal, D. Gaskell, T. Gautam, M. Gericke, C. Ghosh, I. Halilovic, J.-O. Hansen, F. Hauenstein, W. Henry, C. J. Horowitz, C. Jantzi, S. Jian, S. Johnston, D. C. Jones, B. Karki, S. Katugampola, C. Keppel, P. M. King, D. E. King, M. Knauss, K. S. Kumar, T. Kutz, N. Lashley-Colthirst, G. Leverick, H. Liu, N. Liyanage, S. Malace, R. Mammei, J. Mammei, M. McCaughan, D. McNulty, D. Meekins, C. Metts, R. Michaels, M. M. Mondal, J. Napolitano, A. Narayan, D. Nikolaev, M. N. H. Rashad, V. Owen, C. Palatchi, J. Pan, B. Pandey, S. Park, K. D. Paschke, M. Petrusky, M. L. Pitt, S. Premathilake, A. J. R. Puckett, B. Quinn, R. Radloff, S. Rahman, A. Rathnayake, B. T. Reed, P. E. Reimer, R. Richards, S. Riordan, Y. Roblin, S. Seeds, A. Shahinyan, P. Souder, L. Tang, M. Thiel, Y. Tian, G. M. Urciuoli, E. W. Wertz, B. Wojtsekhowski, B. Yale, T. Ye, A. Yoon, A. Zec, W. Zhang, J. Zhang, and X. Zheng (PREX Collaboration), Accurate determination of the neutron skin thickness of ^{208}Pb through parity-violation in electron scattering, *Phys. Rev. Lett.* **126**, 172502 (2021).
- [38] B. T. Reed, F. J. Fattoyev, C. J. Horowitz, and J. Piekarewicz, Implications of prex-2 on the equation of state of neutron-rich matter, *Phys. Rev. Lett.* **126**, 172503 (2021).
- [39] S. Tagami, T. Wakasa, and M. Yahiro, Slope parameters determined from crex and prex2, *Results in Physics* **43**, 106037 (2022).
- [40] N. Wang and T. Li, Shell and isospin effects in nuclear charge radii, *Phys. Rev. C* **88**, 011301 (2013).
- [41] B. A. Brown, K. Minamisono, J. Piekarewicz, H. Hergert, D. Garand, A. Klose, K. König, J. D. Lantis, Y. Liu, B. Maaß, A. J. Miller, W. Nörtershäuser, S. V. Pineda, R. C. Powel, D. M. Rossi, F. Sommer, C. Sumithrarachchi, A. Teigelhöfer, J. Watkins, and R. Wirth, Implications of the $^{36}\text{Ca}-^{36}\text{S}$ and $^{38}\text{Ca}-^{38}\text{Ar}$ difference in mirror charge radii on the neutron matter equation of state, *Phys. Rev. Res.* **2**, 022035 (2020).
- [42] S. V. Pineda, K. König, D. M. Rossi, B. A. Brown, A. Incorvati, J. Lantis, K. Minamisono, W. Nörtershäuser, J. Piekarewicz, R. Powel, and F. Sommer, Charge radius of neutron-deficient ^{54}Ni and symmetry energy constraints using the difference in mirror pair charge radii, *Phys. Rev. Lett.* **127**, 182503 (2021).
- [43] R. An, S. Sun, L.-G. Cao, and F.-S. Zhang, Constraining nuclear symmetry energy with the charge radii of mirror-pair nuclei, *Nuclear Science and Techniques* **34**, 119 (2023).
- [44] Y. N. Huang, Z. Z. Li, and Y. F. Niu, Correlation between the difference of charge radii in mirror nuclei and the slope parameter of the symmetry energy, *Phys. Rev. C* **107**, 034319 (2023).
- [45] T. Li, Y. Luo, and N. Wang, Compilation of recent nuclear ground state charge radius measurements and tests for models, *Atomic Data and Nuclear Data Tables* **140**, 101440 (2021).
- [46] A. Trzcińska, J. Jastrzębski, P. Lubiński, F. J. Hartmann, R. Schmidt, T. von Egidy, and B. Klos, Neutron density distributions deduced from antiprotonic atoms, *Phys. Rev. Lett.* **87**, 082501 (2001).
- [47] S. J. Novario, D. Lonardonì, S. Gandolfi, and G. Hagen, Trends of neutron skins and radii of mirror nuclei from first principles, *Phys. Rev. Lett.* **130**, 032501 (2023).
- [48] W. D. Myers and W. Swiatecki, Average nuclear properties, *Annals of Physics* **55**, 395 (1969).
- [49] W. Myers and W. Swiatecki, The nuclear droplet model for arbitrary shapes, *Annals of Physics* **84**, 186 (1974).
- [50] W. Myers and W. Swiatecki, Droplet-model theory of the neutron skin, *Nuclear Physics A* **336**, 267 (1980).
- [51] C. Pethick and D. Ravenhall, The dependence of neutron skin thickness and surface tension on neutron excess, *Nuclear Physics A* **606**, 173 (1996).
- [52] J. Zenihiro, H. Sakaguchi, S. Terashima, T. Uesaka, G. Hagen, M. Itoh, T. Murakami, Y. Nakatsugawa, T. Ohnishi, H. Sagawa, H. Takeda, M. Uchida, H. P. Yoshida, S. Yoshida, and M. Yosoi, Direct determination of the neutron skin thicknesses in $^{40,48}\text{Ca}$ from proton elastic scattering at $e_p = 295$ mev (2018), [arXiv:1810.11796 \[nucl-ex\]](https://arxiv.org/abs/1810.11796).
- [53] J. JASTRZEBSKI, A. TRZCIŃSKA, P. LUBIŃSKI, B. KLOS, F. J. HARTMANN, T. von EGIDY, and S. WYCECH, Neutron density distributions from antiprotonic atoms compared with hadron scattering data, *International Journal of Modern Physics E* **13**, 343 (2004), <https://doi.org/10.1142/S0218301304002168>.
- [54] W. R. Gibbs and J.-P. Dedonder, Neutron radii of the calcium isotopes, *Phys. Rev. C* **46**, 1825 (1992).
- [55] D. Adhikari, H. Albatineh, D. Androic, K. A. Aniol, D. S. Armstrong, T. Averett, C. Ayerbe Gayoso, S. K. Barcus, V. Bellini, R. S. Beminiwattha, J. F. Benesch, H. Bhatt, D. Bhatta Pathak, D. Bhetuwal, B. Blaikie, J. Boyd, Q. Campagna, A. Camsonne, G. D. Cates, Y. Chen, C. Clarke, J. C. Cornejo, S. Covrig Dusa, M. M. Dalton, P. Datta, A. Deshpande, D. Dutta, C. Feldman, E. Fuchey, C. Gal, D. Gaskell, T. Gautam, M. Gericke, C. Ghosh, I. Halilovic, J.-O. Hansen, O. Hassan, F. Hauenstein, W. Henry, C. J. Horowitz, C. Jantzi, S. Jian, S. Johnston, D. C. Jones, S. Kakkar, S. Katugampola, C. Keppel, P. M. King, D. E. King, K. S. Kumar, T. Kutz, N. Lashley-Colthirst, G. Leverick, H. Liu, N. Liyanage, J. Mammei, R. Mammei, M. McCaughan, D. McNulty, D. Meekins, C. Metts, R. Michaels, M. Mihovilovic, M. M. Mondal, J. Napolitano, A. Narayan, D. Nikolaev, V. Owen, C. Palatchi, J. Pan, B. Pandey, S. Park, K. D. Paschke, M. Petrusky, M. L. Pitt, S. Premathilake, B. Quinn, R. Radloff, S. Rahman, M. N. H. Rashad, A. Rathnayake, B. T. Reed, P. E. Reimer, R. Richards, S. Riordan, Y. R. Roblin, S. Seeds, A. Shahinyan, P. Souder, M. Thiel, Y. Tian, G. M. Urciuoli, E. W. Wertz, B. Wojtsekhowski, B. Yale, T. Ye, A. Yoon, W. Xiong, A. Zec, W. Zhang, J. Zhang, and X. Zheng (CREX Collaboration), Precision determination of the neutral weak form factor of ^{48}Ca , *Phys. Rev. Lett.* **129**, 042501 (2022).
- [56] G. Giacalone, G. Nijs, and W. van der Schee, Determination of the neutron skin of ^{208}Pb from ultrarelativistic nuclear collisions, *Phys. Rev. Lett.* **131**, 202302 (2023).
- [57] D. Adhikari, H. Albatineh, D. Androic, K. Aniol, D. S. Armstrong, T. Averett, C. Ayerbe Gayoso, S. Barcus,

- V. Bellini, R. S. Beminiwattha, J. F. Benesch, H. Bhatt, D. Bhatta Pathak, D. Bhetuwal, B. Blaikie, Q. Campaigna, A. Camsonne, G. D. Cates, Y. Chen, C. Clarke, J. C. Cornejo, S. Covrig Dusa, P. Datta, A. Deshpande, D. Dutta, C. Feldman, E. Fuchey, C. Gal, D. Gaskell, T. Gautam, M. Gericke, C. Ghosh, I. Halilovic, J.-O. Hansen, F. Hauenstein, W. Henry, C. J. Horowitz, C. Jantzi, S. Jian, S. Johnston, D. C. Jones, B. Karki, S. Katugampola, C. Keppel, P. M. King, D. E. King, M. Knauss, K. S. Kumar, T. Kutz, N. Lashley-Colthirst, G. Leverick, H. Liu, N. Liyange, S. Malace, R. Mammei, J. Mammei, M. McCaughan, D. McNulty, D. Meekins, C. Metts, R. Michaels, M. M. Mondal, J. Napolitano, A. Narayan, D. Nikolaev, M. N. H. Rashad, V. Owen, C. Palatchi, J. Pan, B. Pandey, S. Park, K. D. Paschke, M. Petrusky, M. L. Pitt, S. Premathilake, A. J. R. Puckett, B. Quinn, R. Radloff, S. Rahman, A. Rathnayake, B. T. Reed, P. E. Reimer, R. Richards, S. Riordan, Y. Roblin, S. Seeds, A. Shahinyan, P. Souder, L. Tang, M. Thiel, Y. Tian, G. M. Urciuoli, E. W. Wertz, B. Wojtsekhowski, B. Yale, T. Ye, A. Yoon, A. Zec, W. Zhang, J. Zhang, and X. Zheng (PREX Collaboration), Accurate determination of the neutron skin thickness of ^{208}Pb through parity-violation in electron scattering, *Phys. Rev. Lett.* **126**, 172502 (2021).
- [58] A. Alexandrovich, A. Gagarski, I. Krasnoschekova, G. Petrov, V. Petrova, A. Petukhov, Y. Pleva, P. Geltenbort, J. Last, and K. Schreckenbach, New observation of space-parity violation in neutron-induced fission of 229th, 241pu and 241am, *Nuclear Physics A* **567**, 541 (1994).
- [59] L. Ray, Neutron isotopic density differences deduced from 0.8 gev polarized proton elastic scattering, *Phys. Rev. C* **19**, 1855 (1979).
- [60] G. W. Hoffmann, L. Ray, M. Barlett, J. McGill, G. S. Adams, G. J. Igo, F. Irom, A. T. M. Wang, C. A. Whitten, R. L. Boudrie, J. F. Amann, C. Glashauser, N. M. Hintz, G. S. Kyle, and G. S. Blanpied, 0.8 gev $p+^{208}\text{Pb}$ elastic scattering and the quantity Δr_{np} , *Phys. Rev. C* **21**, 1488 (1980).
- [61] S. Abrahamyan, Z. Ahmed, H. Albatineh, K. Aniol, D. S. Armstrong, W. Armstrong, T. Averett, B. Babineau, A. Barbieri, V. Bellini, R. Beminiwattha, J. Benesch, F. Benmokhtar, T. Bielarski, W. Boeglin, A. Camsonne, M. Canan, P. Carter, G. D. Cates, C. Chen, J.-P. Chen, O. Hen, F. Cusanno, M. M. Dalton, R. De Leo, K. de Jager, W. Deconinck, P. Decowski, X. Deng, A. Deur, D. Dutta, A. Etile, D. Flay, G. B. Franklin, M. Friend, S. Frullani, E. Fuchey, F. Garibaldi, E. Gasser, R. Gilman, A. Giusa, A. Glamazdin, J. Gomez, J. Grames, C. Gu, O. Hansen, J. Hansknecht, D. W. Higinbotham, R. S. Holmes, T. Holmstrom, C. J. Horowitz, J. Hoskins, J. Huang, C. E. Hyde, F. Itard, C.-M. Jen, E. Jensen, G. Jin, S. Johnston, A. Keller, K. Kliakhandler, P. M. King, S. Kowalski, K. S. Kumar, J. Leacock, J. Leckey, J. H. Lee, J. J. LeRose, R. Lindgren, N. Liyanage, N. Lubinsky, J. Mammei, F. Mammoliti, D. J. Margaziotis, P. Markowitz, A. McCreary, D. McNulty, L. Mercado, Z.-E. Meziani, R. W. Michaels, M. Mihovilovic, N. Muangma, C. Muñoz Camacho, S. Nanda, V. Nelyubin, N. Nuruzzaman, Y. Oh, A. Palmer, D. Parno, K. D. Paschke, S. K. Phillips, B. Poelker, R. Pomatsalyuk, M. Posik, A. J. R. Puckett, B. Quinn, A. Rakhman, P. E. Reimer, S. Riordan, P. Rogan, G. Ron, G. Russo, K. Saenboonruang, A. Saha, B. Sawatzky, A. Shahinyan, R. Silwal, S. Sirca, K. Slifer, P. Solvignon, P. A. Souder, M. L. Sperduto, R. Subedi, R. Suleiman, V. Sulkosky, C. M. Sutura, W. A. Tobias, W. Troth, G. M. Urciuoli, B. Waidyawansa, D. Wang, J. Wexler, R. Wilson, B. Wojtsekhowski, X. Yan, H. Yao, Y. Ye, Z. Ye, V. Yim, L. Zana, X. Zhan, J. Zhang, Y. Zhang, X. Zheng, and P. Zhu (PREX Collaboration), Measurement of the neutron radius of ^{208}Pb through parity violation in electron scattering, *Phys. Rev. Lett.* **108**, 112502 (2012).
- [62] I. Angeli and K. Marinova, Table of experimental nuclear ground state charge radii: An update, *Atomic Data and Nuclear Data Tables* **99**, 69 (2013).
- [63] V. Kota, Embedded random matrix ensembles for complexity and chaos in finite interacting particle systems, *Physics Reports* **347**, 223 (2001).
- [64] V. Zelevinsky and A. Volya, Nuclear structure, random interactions and mesoscopic physics, *Physics Reports* **391**, 311 (2004), from atoms to nuclei to quarks and gluons: the omnipresent manybody theory.
- [65] Y. Zhao, A. Arima, and N. Yoshinaga, Regularities of many-body systems interacting by a two-body random ensemble, *Physics Reports* **400**, 1 (2004).
- [66] H. A. Weidenmüller and G. E. Mitchell, Random matrices and chaos in nuclear physics: Nuclear structure, *Rev. Mod. Phys.* **81**, 539 (2009).
- [67] B. Sherrill and R. F. Casten, Future articles: Frontiers of nuclear structure: Exotic nuclei, *Nuclear Physics News* **15**, 13 (2005), <https://doi.org/10.1080/10506890500454675>.
- [68] C. W. Johnson, G. F. Bertsch, and D. J. Dean, Orderly spectra from random interactions, *Phys. Rev. Lett.* **80**, 2749 (1998).
- [69] Y. M. Zhao, A. Arima, N. Shimizu, K. Ogawa, N. Yoshinaga, and O. Scholten, Patterns of the ground states in the presence of random interactions: Nucleon systems, *Phys. Rev. C* **70**, 054322 (2004).
- [70] R. Bijker and A. Frank, Band structure from random interactions, *Phys. Rev. Lett.* **84**, 420 (2000).
- [71] J. J. Shen, H. Jiang, and G. J. Fu, Robustness of “noncollective” rotational behavior for nuclei in the presence of random interactions, *Phys. Rev. C* **104**, 054319 (2021).
- [72] G. J. Fu, J. J. Shen, Y. M. Zhao, and A. Arima, Regularities in low-lying states of atomic nuclei with random interactions, *Phys. Rev. C* **91**, 054319 (2015).
- [73] Y. Lei, Robust correlations between quadrupole moments of low-lying 2^+ states within random-interaction ensembles, *Phys. Rev. C* **93**, 024319 (2016).
- [74] Z.-Z. Qin and Y. Lei, Predominance of linear q and μ systematics in random-interaction ensembles, *Nuclear Science and Techniques* **29**, 163 (2018).
- [75] C. W. Johnson, W. E. Ormand, K. S. McElvain, and H. Shan, *Bigstick: A flexible configuration-interaction shell-model code* (2018), [arXiv:1801.08432 \[physics.comp-ph\]](https://arxiv.org/abs/1801.08432).
- [76] P. Karl, VII. note on regression and inheritance in the case of two parents, *Proc. R. Soc. Lond.* **58**, 240 (1895).
- [77] P. Marevic, N. Schunck, E. Ney, R. Navarro Perez, M. Verriere, and J. O’Neal, Axially-deformed solution of the skyrme-hartree-fock-bogoliubov equations using the transformed harmonic oscillator basis (iv) hfbtho (v4.0): A new version of the program, *Computer Physics Communications* **276**, 108367 (2022).

- [78] M. Dutra, O. Lourenço, J. S. Sá Martins, A. Delfino, J. R. Stone, and P. D. Stevenson, Skyrme interaction and nuclear matter constraints, *Phys. Rev. C* **85**, 035201 (2012).
- [79] L. Devroye, Multivariate distributions, in *Non-Uniform Random Variate Generation* (Springer New York, New York, NY, 1986) pp. 554–610.
- [80] H. Kohler, Skyrme force and the mass formula, *Nuclear Physics A* **258**, 301 (1976).
- [81] K. Heyde and J. L. Wood, Shape coexistence in atomic nuclei, *Rev. Mod. Phys.* **83**, 1467 (2011).
- [82] Y. Lei, J. Qi, Y. Lu, H. Jiang, Z. Z. Qin, D. Liu, and C. W. Johnson, Pervasiveness of shape coexistence in nuclear pair condensates, *Phys. Rev. C* **110**, 054318 (2024).